

Oxygen Reduction Reaction on Pt-Y/C Catalysts: Activity and Long-Term Stability Study

Gabriel Christiano da Silva *^a and Joelma Perez^b

^a*Instituto de Química, Universidade Federal da Bahia (UFBA), Campus Universitário de Ondina, 40170-115 Salvador-BA, Brazil*

^b*Instituto de Química de São Carlos, Universidade de São Paulo (USP), CP 780, 13560-970 São Carlos-SP, Brazil*

Pt-Y/C catalysts were prepared by a modified formic acid method and their structural characteristics and activity for oxygen reduction reaction (ORR) were evaluated. X-ray diffraction analysis showed that no alloy was formed between the metals and X-ray photoelectron spectroscopy (XPS) experiments showed that yttrium is presented as Y_2O_3 , $\text{Y}(\text{OH})_3$ and $\text{Y}-\text{O}-\text{Pt}$ species. CO stripping voltammetry and *in situ* X-ray absorption spectroscopy confirmed the interaction between Pt nanoparticles and yttrium species. The Pt-Y/C 7:3 material showed the higher specific activity ($103 \mu\text{A cm}_{\text{Pt}}^{-2}$) for ORR. Following repetitive potential cycling, the activity for the ORR of the Pt-Y/C 7:3 catalyst declined in a similar proportion to the Pt/C material. Transmission electron microscopy analysis after stability for both catalysts showed that Pt/C particle size slightly increased and that for Pt-Y/C 7:3 remained the same. XPS made in ultrathin catalyst layer, agreeing with energy-dispersive X-ray spectroscopy analysis, revealed that the intensities of the Y 3d peaks were suppressed relative to the initial one and that yttrium in the form of Y_2O_3 and $\text{Y}(\text{OH})_3$ were dissolved, while the species $\text{Y}-\text{O}-\text{Pt}$ still remain in the catalyst, maintaining the higher activity.

Keywords: Pt-Y/C, yttrium, platinum, oxygen reduction, fuel cell, stability

Introduction

In the last few years, significant improvements have been made to polymer electrolyte membrane full cells (PEMFC) and they are currently considered a promising alternative energy technology.^{1,2} Despite the progress reached, the oxygen reduction reaction (ORR), which takes place at the cathode of the PEMFC, stills as the major obstacle for the full utilization of these devices. Consequently, significant effort has been made in the development of electrocatalyst materials that combine high activity and good stability for the ORR in the operating conditions of the PEMFC.³⁻⁷

Greeley *et al.*⁸ making use of density functional theory (DFT), studied the ORR activity and stability of Pt_3M (M = transition metals) alloys. The computational results showed that Pt alloyed with early transition metals, such as Y, are more active and stable than pure Pt. In addition, electrochemical measurements of Pt_3Y sputtering electrode revealed an activity enhancement by a factor of 6, in the potential of 0.9 V, compared with pure Pt.

Several subsequent studies^{9,10} confirmed the advantages of PtY sputtered alloys both in terms of activity and stability. Nonetheless, the practical application of Pt-Y catalysts in PEMFCs depends on the development of carbon-supported nanoparticles catalysts.

Jeon and McGinn¹¹ synthesized PtY/C and $\text{Pt}_3\text{Y}/\text{C}$ catalysts via the NaBH_4 reduction method. These materials were evaluated for their ORR activity using a rotating disc electrode; an activity increase of 23 and 65% were obtained for the $\text{Pt}_3\text{Y}/\text{C}$ and PtY/C materials, respectively, when compared to Pt/C synthesized using the same method. Nishanth *et al.*¹² evaluated the ORR activity in the presence of methanol of Pt-Y(OH)₃/C catalyst, also obtained by NaBH_4 reduction. These bimetallic catalysts had higher activity and selectivity for ORR compared to Pt/C. A direct methanol fuel cell operating with Pt-Y(OH)₃/C as the cathode catalyst had a better performance than the one in which Pt/C was used. This result confirmed the higher activity for ORR as well as a higher tolerance for methanol crossover.

Recently, Luo *et al.*¹³ synthesized Pt-rare earth catalyst via a water-in-oil chemical route. The authors reported a higher activity towards ORR for Pt-Y₂O₃/C catalysts compared to the activity of Pt/C and Pt-Gd₂O₃/C materials.

*e-mail: gabrielchristiano@ufba.br

Editor handled this article: Rodrigo A. A. Muñoz (Associate)

In another paper,¹⁴ the same authors described that the specific activity of the as prepared Pt-Y₂O₃/C catalyst did not change after 6000 cycles durability test.

Considering the above-mentioned studies, Pt-Y materials appear to be extremely efficient catalysts for the ORR and are promising substitutes for pure Pt catalysts for use as PEMFC cathodes. To date few studies have been made using carbon-supported Pt-Y catalyst. Besides, changes in the particle size and its composition after the stability test were not evaluated. In this contribution a modified formic acid method was employed to obtain Pt-Y/C catalysts. The catalysts activities toward ORR were studied and their stability evaluated in a new way employing the energy-dispersive X-ray spectroscopy (EDS) and X-ray photoelectron spectroscopy (XPS) techniques directly on the catalyst layer of the electrode.

Experimental

Pt-Y/C catalysts synthesis

Carbon supported Pt-Y (20 wt.%) catalyst, with metal atomic proportions of 1:1, 7:3 and 9:1, were prepared by employing formic acid as reducing agent. The use of traditional formic acid synthesis method¹⁵ did not result in obtaining the desired Pt-Y/C catalysts compositions. dos Santos *et al.*¹⁶ reported the impossibility in obtaining Pt-Ru/C catalyst with ruthenium atomic content higher than 25% through formic acid method. After increasing the pH of the synthesis, ruthenium atomic contents of 35 and 60% were obtained for pH values equal to 10 and 14, respectively. Therefore, pH modification was also used here. In the conventional synthesis,¹⁵ the carbon support (Vulcan XC72R, Cabot Corporation, Boston, MA, USA) is dispersed in a 0.5 mol L⁻¹ formic acid solution (Merck, Darmstadt, Germany). In this case, a modification was made by increasing the dispersion pH to 12.5 through the addition of potassium hydroxide pellets (Panreac, Barcelona, Spain). In sequence, the solution temperature was raised to 80 °C under argon atmosphere. The metallic precursors chloroplatinic acid hexahydrate (H₂PtCl₆.6H₂O, Sigma-Aldrich, St. Louis, MO, USA) and yttrium(III) chloride hexahydrate (YCl₃.6H₂O, Sigma-Aldrich, St. Louis, MO, USA) were added to the solution, in the appropriate proportions, while stirring. After a period of 15 min, the solution was allowed to cool to room temperature and the resulting supported catalyst was then filtered and washed with water. The synthesized electrocatalysts were named Pt-Y/C 1:1, Pt-Y/C 7:3 and Pt-Y/C 9:1.

Since ORR is sensitive to the particle size,¹⁷⁻¹⁹ the Pt-Y/C electrocatalysts activities were compared to a

commercial Pt/C (Etek, 20%, Milan, Italy) submitted to a thermal treatment under argon atmosphere at 500 °C for 3 h, which had a similar mean particle size.

Catalysts characterization

Platinum and yttrium contents of the electrocatalyst were determined by EDS analysis performed in a Leica-Zeiss LEO 440 scanning electron microscope (SEM, Leica-Zeiss, Jena, Germany) with an electron beam acceleration voltage of 20 keV.

X-ray diffraction (XRD) was used to analyze the crystal structure of the supported catalysts. The diffractograms were obtained at a scan rate of 1° min⁻¹ for 2θ values between 10 and 100° using a Rigaku Ultima IV diffractometer (Rigaku, Tokyo, Japan) operating with Cu Kα radiation (1.5406 Å).

The mean particle size and particle distribution was characterized using transmission electron microscopy (TEM). The micrographs were obtained using a JEOL JEM2100 (JEOL, Tokyo, Japan) instrument operating at an accelerating voltage of 200 kV.

XPS studies were carried out at the Laboratório Nacional de Nanotecnologia (LNNano, Campinas, Brazil) using a Thermo Scientific™ K-AlphaTM+ (Thermo Fisher Scientific, Waltham, MA, USA) spectrometer equipped with an aluminum monochromator, an X-ray energy of 1487 eV (Al Kα), and pass energy of 20 eV. The energy was calibrated to give a Au 4f_{7/2} metallic gold signal at 84 eV. The equipment was programmed to provide a spot size of 400 μm, while the spectra were acquired with an energy step of 0.1 eV and an acquisition time of 200 ms.

The *in situ* X-ray absorption spectroscopy (XAS) was performed at the Laboratório Nacional de Luz Síncrotron (LNLS, Campinas, Brazil) using a homemade spectroelectrochemical cell in the transmission mode.²⁰ The working electrode consisted of a 6 mg_{Pt} cm⁻² catalysts pellet mixed with 35.5 wt.% Nafion solution (Dupont, 6 wt.%, Wilmington, DE, USA). The reference electrode consisted of a reversible hydrogen electrode and a Pt screen, cut in the center to allow the free passage of X-ray beam, was used as counter electrode. The measurements were carried out in 0.5 mol L⁻¹ H₂SO₄ (Panreac, Barcelona, Spain) and 700 mV *vs.* reversible hydrogen electrode (RHE). The XAS spectra were acquired on the Pt L_{III} edge (11.564 keV) and the scans were performed from 11.440 to 12.200 keV.

Electrochemical measurements

Electrochemical characterizations of the synthesized catalyst were performed within a standard glass cell with

the three-electrode configuration. A RHE and a Pt foil were used as reference and counter electrodes, respectively. All potential values herein are reported based on the RHE scale. The working electrode consisted of an ultrathin catalyst layer containing 28 µg of metal cm⁻² deposited on polished glassy carbon electrode in a Teflon sleeve (geometric surface area = 0.196 cm²). The glassy carbon electrode was of the change disk type which allowed the disk removal for catalyst layer subsequent analysis.

The ultrathin catalyst layer was prepared by mixing ultrasonically 1.8 mg of the catalyst, 15 µL of Nafion (Dupont, 6 wt.%, Wilmington, DE, USA), and 1.0 mL isopropyl alcohol (Panreac, Barcelona, Spain). After the mixing, 16 µL of the suspension was uniformly distributed on the surface of the glassy carbon electrode with a microsyringe. All of the electrochemical measurements were carried out in argon-purged 0.5 mol L⁻¹ H₂SO₄ electrolyte (Panreac, Barcelona, Spain), at ambient temperature, using an Autolab PGSTAT302N potentiostat/galvanostat (Metrohm, Herisau, Switzerland) controlled using GPES electrochemical software.

Prior to ORR analysis, cyclic voltammetry (CV) between 0 and 0.8 V at a sweep rate of $v = 50$ mV s⁻¹ was carried out, until a stable CV profile was obtained. After the cleaning, CV profiles were collected between 0 and 1.0 V at a sweep rate of 50 mV s⁻¹ in order to evaluate the electrochemically active surface area (A_{ecsa}) of the platinum. This calculation is performed by integrating the hydrogen desorption peaks from the CV profile, and assuming that the charge for the desorption of one monolayer of hydrogen is equal to 210 µC cm⁻².²¹

The catalytic ORR activities of the Pt-Y/C materials and the Pt/C catalyst were studied employing the rotating disk electrode (RDE) technique.²² Potential sweeps between 0.1 and 1.1 V at a scan rate of 5 mV s⁻¹ and RDE rotation rates of 100, 400, 900, 1600, and 2500 rpm were performed after oxygen saturation of the electrolyte.

The CO stripping voltammetry was performed allowing CO gas to pass in the electrochemical cell for 5 min while the working electrode was kept polarized at 0.1 V. The excess CO was purged using Ar gas for 25 min. The adsorbed CO was oxidized at a scan rate of 5 mV s⁻¹.

Accelerated aging tests were performed by potential cycling of the working electrodes for 3000 cycles between 0.6 and 1.1 V at a sweep rate of 50 mV s⁻¹. After the aging tests, the A_{ecsa} and the ORR activities of the electrocatalysts were re-evaluated. Removing the carbon disk, EDS and XPS techniques were used to analyze the aging effects on catalyst metals contents. For TEM studies the catalyst layer was removed from the disk using isopropyl alcohol.

Results and Discussion

Physicochemical characterization

The EDS analyses of the synthesized electrocatalysts showed Pt:Y atomic ratios equal to 51:49, 71:29 and 88:12. Thus, they are in agreement with the 1:1, 7:3 and 9:1 intend nominal values and confirm the successful incorporation of yttrium into the catalyst.

Figure 1 presents the TEM micrographs. In each case, we observed a homogenous distribution for the electrocatalysts over the carbon support. Mean particle sizes of 5.0, 6.0, and 4.6 nm are obtained for the 1:1, 7:3, and 9:1 bimetallic materials, respectively, while the Pt/C catalyst has a mean particle size of 4.2 nm (Table 1).

The XRD results for the Pt-Y/C electrocatalysts are presented in Figure 2. The carbon support diffraction peak is located at ca. $2\theta = 25^\circ$. The other peaks, in ascending order of 2θ , are related to the reflexions of (111), (200), (220), (311), and (222) platinum fcc crystallographic faces.²³⁻²⁵ The absence of diffraction peaks for species such as Y⁰, Y₂O₃¹¹ and Y(OH)₃²⁶ suggests that the yttrium is present in amorphous form. The mean crystallite sizes (D) and the lattice parameters (a_{exp}) of the catalysts were estimated using Scherrer's equation and Bragg's law,^{27,28} respectively, for the (220) diffraction peaks. The results are presented in Table 1, which also includes Pt-Pt interatomic distances.

The synthesized Pt-Y/C catalysts have an average crystallite size that varies from 4.6 to 6.1 nm, based on the application of the Scherrer equation, and are in agreement with the values of mean particle size from the TEM analysis. These values are similar to the average size of 4.7 and 5.4 nm for the PtY/C and Pt₃Y/C catalysts synthesized by Jeon and McGinn,¹¹ and lower than the 8.4 nm average crystallite size found by Nishanth *et al.*¹² for the Pt-Y(OH)₃/C catalyst.¹²

The lattice parameters can be used to evaluate the degree of alloying in binary materials that follow Vegard's law. As yttrium has an atomic radius that is larger than that of platinum, its incorporation into the crystal structure of Pt would cause an expansion in the lattice spacing (d_{fcc}),²⁹ resulting in larger values for a_{exp} and the translation of XRD diffraction peaks to smaller angles. The a_{exp} and d_{fcc} values for the Pt-Y/C catalysts are similar to the values obtained for the Pt/C. Furthermore, as shown in Figure 2, no translations in the XRD peaks are observed, indicating that no alloy was formed between Pt and Y.

High resolution XPS spectra corresponding to Pt 4f and Y 3d energy states of the electrocatalysts are shown in Figure 3. The Pt 4f spectra can be deconvoluted in three

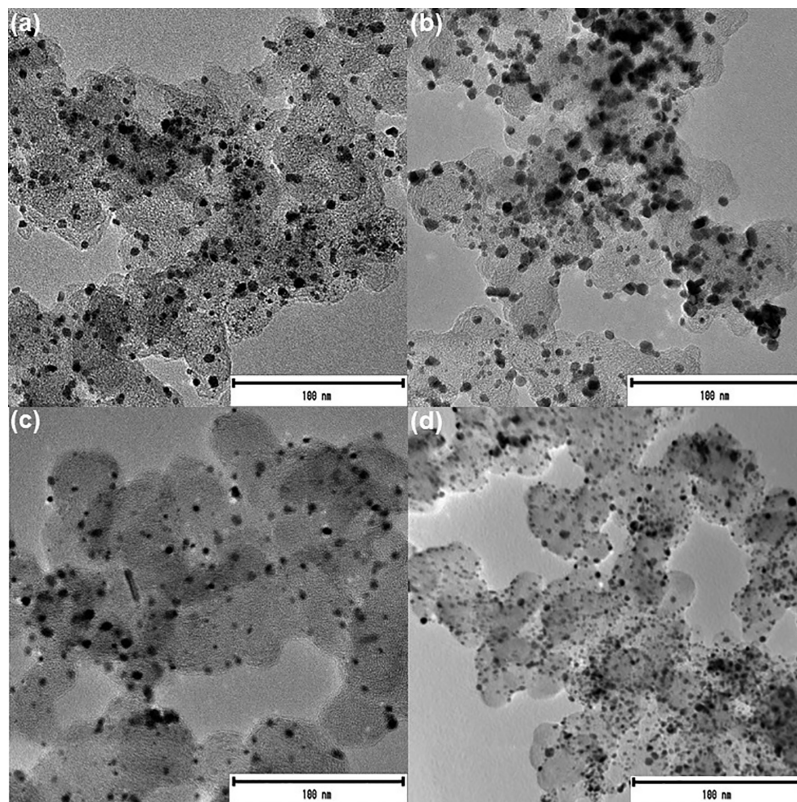


Figure 1. Transmission electron micrographs of Pt-Y/C 1:1 (a), 7:3 (b), 9:1 (c), and Pt/C (d) catalysts.

Table 1. Average crystallite sizes (D), lattice parameters (a_{exp}) Pt-Pt interatomic distance (d_{fcc}) and TEM mean particle size values for Pt/C and Pt-Y/C catalysts

	D / nm	$a_{\text{exp}} / \text{\AA}$	$d_{\text{fcc}} / \text{\AA}$	Particle size (TEM) / nm	
				Initial	Aged
Pt-Y/C 1:1	5.6	3.919	2.771	5.0	—
Pt-Y/C 7:3	6.1	3.915	2.768	6.0	5.9
Pt-Y/C 9:1	4.6	3.923	2.774	4.6	—
Pt/C	5.2	3.924	2.775	4.2	4.6

TEM: transmission electron microscopy.

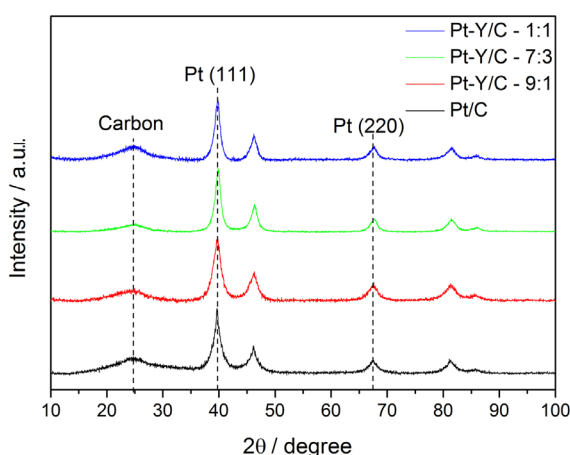


Figure 2. X-ray diffractograms of the synthesized Pt-Y/C catalysts and Pt/C. The vertical lines represent the carbon, Pt (111), and Pt (220) diffraction peaks positions.

sets of doublets peaks. The higher intensity Pt $4f_{7/2}$ peak can be attributed to metallic platinum,³⁰ while the two other Pt $4f_{7/2}$ peaks with energy values close to 72.0 and 74.0 eV are characteristic of the Pt²⁺ and Pt⁴⁺ oxidation states, respectively.

The binding energies related to Pt $4f_{7/2}$ signal of the different Pt oxidation states, as well the percentage value of each one, are given in Table 2. The values in brackets show that the platinum compositions of the Pt-Y/C synthesized catalyst are similar to that in Pt/C material. Almost 60% of surface platinum is found in the metallic form, while 30% and 10% are in the +2 and +4 oxidation states, respectively.

The Y 3d spectra for all of the Pt-Y/C catalysts indicate that yttrium is present in an oxidized form since there is no peak with binding energy value of 156.0 eV, corresponding

to metallic Y.³¹ The Pt-Y/C 1:1 and 7:3 XPS spectra can be deconvoluted in three sets of doublets peaks. The first Y 3d_{5/2} doublet with binding energy close to 158.0 eV is assigned to Y–O bonding in Y₂O₃. The nominal value for Y 3d_{5/2} in Y₂O₃ is 156.8 eV;^{31,32} so the binding energies corresponding to this oxidation state of both materials exhibit a positive chemical shift greater than 1 eV.

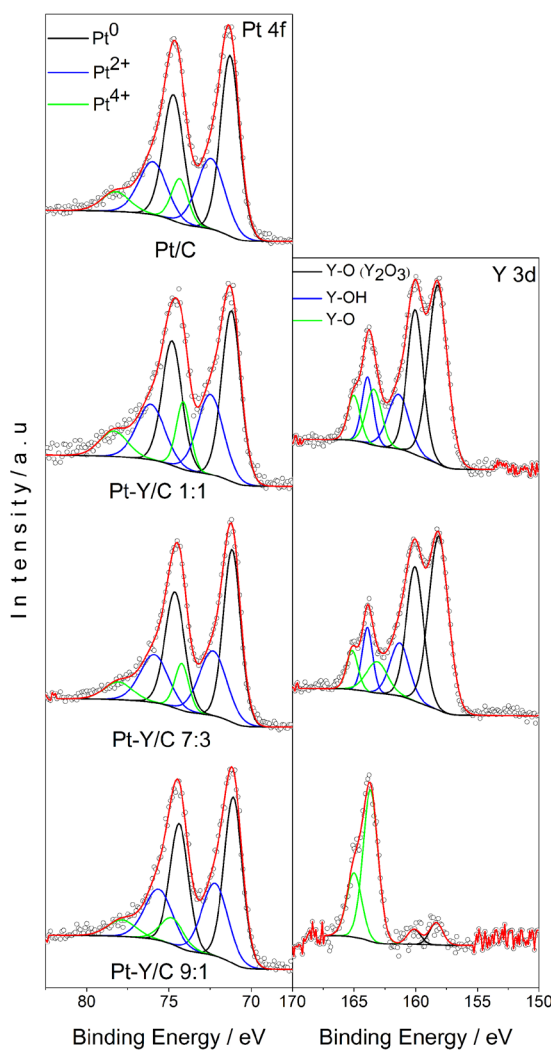


Figure 3. High resolution XPS spectra corresponding to the Pt 4f and Y 3d orbitals of the Pt-Y/C and Pt/C electrocatalysts.

Table 2. Pt 4f_{7/2} and Y 3d_{5/2} binding energy values and atomic percentage of platinum and yttrium species present at each oxidation state for the Pt-Y/C and Pt/C catalysts

Catalyst	Binding energy / eV							XPS ratio / at%
	Pt ⁰	Pt ²⁺ Pt(OH) ₂	Pt ⁴⁺ PtO ₂ .nH ₂ O	Y–O Y ₂ O ₃	Y–OH Y(OH) ₃	Y–O		
Pt-Y/C 1:1	71.2; (52)	72.5; (33)	74.1; (15)	158.2; (63)	161.4; (21)	163.4; (16)		56:44
Pt-Y/C 7:3	71.2; (55)	72.3; (33)	74.2; (12)	158.1; (67)	161.4; (20)	163.1; (13)		66:34
Pt-Y/C 9:1	71.1; (55)	72.2; (34)	74.8; (11)	158.3; (13)	—	163.7; (87)		81:19
Pt/C	71.3; (55)	72.4; (33)	74.3; (12)	—	—	—		

XPS: X-ray photoelectron spectroscopy. Atomic percentage in parenthesis.

Gougousi and Chen³² studied the deposition of yttrium oxide in thin films; a positive chemical shift of 1.8 eV with respect to the nominal value of Y 3d peaks in Y₂O₃ was observed and justified by the explanation that yttrium could be bound to a more electronegative element, such as silicon. In our system, yttrium can react with carbon in the form of carbon dioxide and environmental humidity to produce species that result in shifting of the Y binding energy values.

The second doublet in Pt-Y/C 1:1 and 7:3 XPS spectra is related to Y–OH bonding in Y(OH)₃.³¹ The binding energy values of these Y 3d_{5/2} peaks for both materials are 161.4 eV, which correspond to a positive chemical shift of 2.5 eV as compared to the nominal value of 158.9 eV. The third species in Y 3d Pt-Y/C 1:1 and 7:3 XPS spectra has a Y 3d_{5/2} binding energy value close to 163.0 eV. Ting *et al.*³³ attributed this third doublet to the formation of Y–O–X type bonding, where the X atom is more electronegative than Y but with a similar ionic radius.³³ Yttrium(III) and Pt²⁺ have atomic radii equal to 0.90 and 0.94 Å, respectively. Additionally, Pt is more electronegative (electronegativity value of 2.28) than Y (1.22); so, Y–O–Pt bonding is a possible explanation for the appearance of the third doublet in the XPS spectra.

The XPS spectrum of the Pt-Y/C 9:1 catalyst is quite different from the others. This spectrum could be deconvoluted in only two sets of doublets; no peaks related to Y(OH)₃ were observed. Also, the Y 3d peaks corresponding to Y₂O₃ bonding are less intense for this material, making the third yttrium component (Y–O–X) the principal component of this catalyst. Table 2 summarizes Y 3d_{5/2} binding energies and atomic percentages of the Y components for the bimetallic catalysts.

The catalyst surface composition can be obtained through comparison of the Pt 4f and Y 3d XPS peak area ratio. The yttrium surface content for catalysts 1:1, 7:3 and 9:1 are 44, 34 and 19%, respectively. These values are close to the values of the bulk composition obtained by EDS.

Electrochemical results

Catalysts voltammetric profiles are shown in Figure 4. The hydrogen adsorption/desorption processes taking place at potential values in the 0.0–0.4 V range are characteristics of Pt and have the highest current values corresponding to the Pt-Y/ 9:1 and Pt/C catalysts. The lower platinum surface content and greater particle size of Pt-Y/C 1:1 and 7:3 materials are the main reasons for the lower current in the H₂ potential region for these catalysts. The electrochemically active surface area (A_{ecsa}) was calculated from the voltammograms assuming a 210 μC cm_{pt}⁻² charge for desorption of one monolayer of H₂.²¹ The A_{ecsa} results are presented in Table 3.

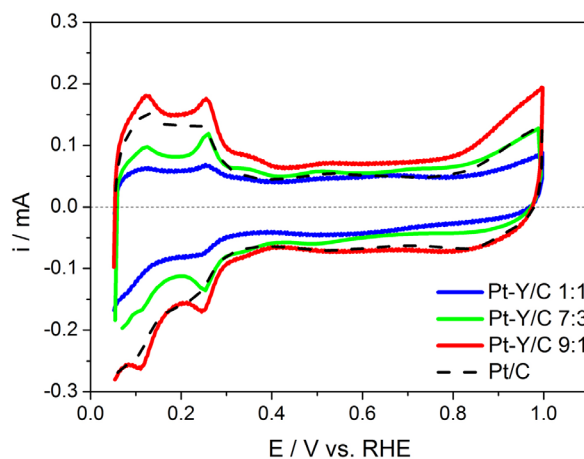


Figure 4. Cyclic voltammograms of Pt-Y/C materials performed in argon purged H₂SO₄ 0.5 M and scan rate of 50 mV s⁻¹.

Figure 5a shows the ORR polarization curves at a rotation speed of 1600 rpm. The inset graph represents the difference in ORR activity in the negative and positive sweep direction for Pt/C catalyst. Although the negative-going sweep is only shown for the Pt/C material, the activity is always higher for the positive going sweep. The Pt-Y/C catalysts with metallic ratio 9:1 and 7:3 exhibited an onset potential of ca. 1 V, similar to that of Pt/C. In the case of Pt-Y/C 1:1, the onset potential is lower, ca. 0.95 V.

A detailed investigation of ORR mechanism for synthesized Pt-Y/C material can be done by employing

Koutecky-Levich equation represented in equation 1:

$$\frac{1}{i} = \frac{1}{i_k} + \frac{1}{i_L} \quad (1)$$

where i_k is the kinetic current and i_L is the limiting current giving by equation 2.²²

$$i_L = 0.62nFAD^{2/3}v^{-1/6}\omega^{1/2}Co^0 \quad (2)$$

where n is the number of electrons involved in ORR, F is Faraday's constant (96,485.3 C mol⁻¹), A is the electrode area (0.196 cm²), D is the oxygen diffusion coefficient (1.4 × 10⁻⁵ cm² s⁻¹), v is the kinematic viscosity of the electrolyte (1.19 × 10⁻² cm² s⁻¹), ω is the electrode angular velocity and C_o⁰ is oxygen solubility (1.10 × 10⁻⁶ mol cm⁻³). Replacing equation 2 in equation 1, Koutecky-Levich equation can be written as:²²

$$\frac{1}{i} = \frac{1}{i_k} + \frac{1}{0.62nFAD^{2/3}v^{-1/6}\omega^{1/2}Co^0} \quad (3)$$

Therefore, the number of electrons transferred during the process, n, can be obtained from the slope of a 1/i vs. 1/ω^{1/2} plot. Koutecky-Levich diagrams are presented in Figure 5b. The curves for the different catalysts have similar slopes indicating that ORR proceeds through the same mechanism. The calculated number of electrons for Pt-Y/C 1:1 material is equal to 3.5, indicating some peroxide formation and justifying the difference in the limiting current in Figure 5a. For the others electrocatalysts, the calculated number of electrons is close to four, suggesting that the ORR may take place via a direct mechanism or through an indirect four-electron mechanism, upon H₂O₂ formation and reduction.

Table 3 summarizes the current density values calculated from 1600 rpm data at 0.9 V. Current values normalized by electrode geometric area (j and j_k) and the mass activity (j_{k-mass}) exhibited by the Pt-Y/C 9:1 catalyst are similar to those of Pt/C material, while increasing the yttrium content of the electrocatalysts those current values decrease. With regard to the specific activity (j_{k-esp}), the current normalized

Table 3. Summary of current density values obtained at 0.9 V and rotation velocity of 1600 rpm

	A _{ecsa} / cm _{pt} ²	j / (mA cm ⁻²)	j _k / (mA cm ⁻²)	j _{k-mass} / (mA mg _{pt} ⁻¹)	j _{k-esp} / (μA cm _{pt} ⁻²)
Pt-Y/C 1:1	0.45	0.05	0.05	3	23
Pt-Y/C 7:3	0.92	0.44	0.48	21	103
Pt-Y/C 9:1	2.13	0.72	0.85	32	78
Pt/C	1.87	0.71	0.83	30	88

A_{ecsa}: electrochemically active surface area; j: current density; j_k: kinetic current; j_{k-mass}: mass activity; j_{k-esp}: specific activity.

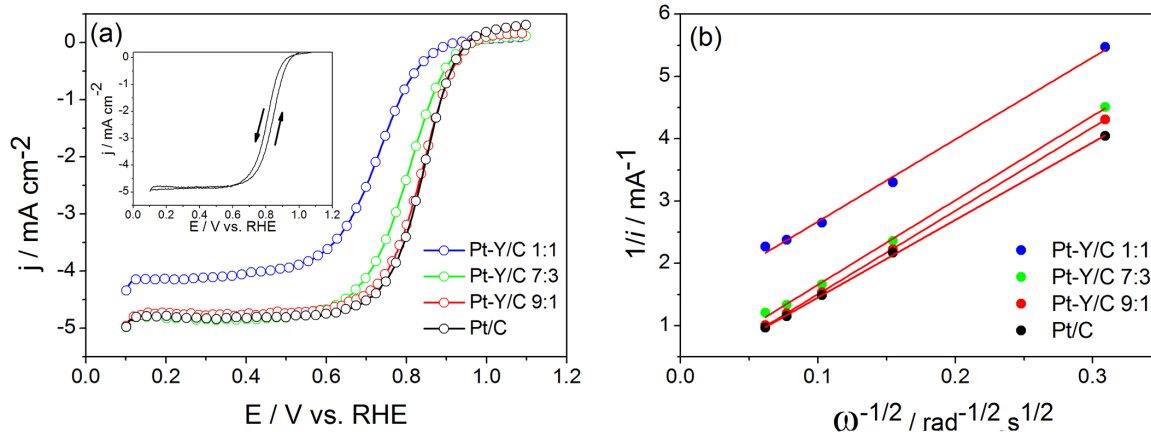


Figure 5. ORR polarization curves for Pt-Y/C and Pt/C catalysts performed at a rotation speed of 1600 rpm and scan rate of 5 mV s^{-1} (a). Inset represents the difference between positive and negative sweep polarization curves obtained for Pt/C material. Koutecky-Levich diagrams obtained at the potential of 720 mV for Pt-Y/C and Pt/C catalysts (b).

by A_{ccsa} , while Pt-Y/C 1:1 and 9:1 display lower current density values, Pt-Y/C 7:3 exhibited a higher $j_{k-\text{esp}}$ value ($103 \mu\text{A cm}_{\text{Pt}}^{-2}$) compared to Pt/C ($88 \mu\text{A cm}_{\text{Pt}}^{-2}$), an increase of almost 20%. However, while those values are superior compared to others Pt-Y₂O₃ catalysts reported in literature, as discussed below, even higher ORR activities can be achieved for Pt-Y bimetallic alloyed nanoparticles.³⁴⁻³⁶

In the work of Jeon and McGinn,¹¹ the catalysts Pt-Y/C (75:25) exhibits a current density of 3.03 mA cm^{-2} at 0.75 V. This value is slightly higher than the current density obtained for the Pt/C synthesized by the same method. The current density for the Pt-Y/C 7:3 catalyst synthesized in this work is 15% higher (3.44 mA cm^{-2}), even with a lower platinum content and higher crystallite size. The authors also report a specific activity of $1050 \mu\text{A cm}_{\text{Pt}}^{-2}$ for the PtY/C-900 catalyst at 0.75V. At the same potential, the specific activity for Pt-Y/C 7:3 is $2533 \mu\text{A cm}_{\text{Pt}}^{-2}$.

Compared to the catalyst Pt-Y₂O₃/C synthesized by Luo *et al.*¹³ with Pt:Y ratio close to 2:1, at 0.9 V the authors reported a specific activity of $54.3 \mu\text{A cm}_{\text{Pt}}^{-2}$, which is lower than those found for Pt-Y/C 7:3 and 9:1 in this work. However, all of the chemically-synthesized bimetallic catalysts still have a poor performance compared to sputtering Pt-Y materials.⁸⁻¹⁰

In order to evaluate any interaction between the Pt nanoparticles and yttrium compounds, CO stripping voltammetries were performed. The CO stripping profiles subtracted from a baseline for the Pt-Y/C catalysts are shown in Figure 6a, which also include the CO stripping profile for Pt/C. Whereas a single peak for CO oxidation, centered at 795 mV, is observed for Pt-Y/C 9:1 and Pt/C materials, increasing the Y content in the electrocatalysts resulted in formation of two peaks in the CO stripping profile, and also in the shift of the onset of CO oxidation at lower potentials for Pt-Y/C 7:3 and 1:1. This behavior has been reported

for others Pt-rare earths electrocatalysts. Corradini *et al.*³⁷ observed the formation of multiple CO oxidation peaks for Pt-Pr/C catalysts with varying Pt:Pr ratios.³⁷ The authors also reported the enhancement of CO electro-oxidation of those catalysts reflected on the shift of the onset values for lower potentials. Lin *et al.*³⁸ observed the CO oxidation activity enhancement of Pt-CeO₂/C which was attributed to the strengthened synergistic effect between Pt and CeO₂ caused by the occurrence of the bi-functional mechanism or by any modification on the electronic structure of Pt.³⁸

Yoo *et al.*³⁹ reported the ORR activity for Pt-Y sputtering alloys with varying Pt:Y contents. The kinetic current for the different materials plotted as function of the d-band centers resulted in a volcano plot with the Pt70Y30 electrode as the most active for the ORR due to geometric and electronic interaction between Pt and Y.⁸⁻¹⁰

Changes in the d-band of Pt in Pt-Y/C catalysts were evaluated using the *in situ* X-ray absorption spectroscopy (XAS), since the Pt L_{III} absorption intensity in the X-ray absorption near edge structure (XANES) spectrum, named the white line intensity, can provide a direct measure of Pt 5d-band occupancy. The XANES spectra for the Pt L_{III} edge for Pt-Y/C and Pt/C catalysts are shown in Figure 6b. A decrease in the white line intensity for Pt-Y/C catalysts, which was more pronounced as the yttrium content increases, was observed compared to Pt/C. This result indicates that Pt nanoparticles and yttrium are not separated and the interaction between Y and Pt results in the occupation of Pt 5d-band. Yoo *et al.*³⁹ observed the decrease in the white line intensity of Pt3Y sputtering electrodes compared to Pt/C.¹⁰ The authors suggest that the Pt3Y alloys electrodes can grab oxygenated species slightly, speeding oxygen-splitting reaction.

With the purpose of evaluating the materials stability, the Pt/C and Pt-Y/C 7:3 catalyst were subjected to an

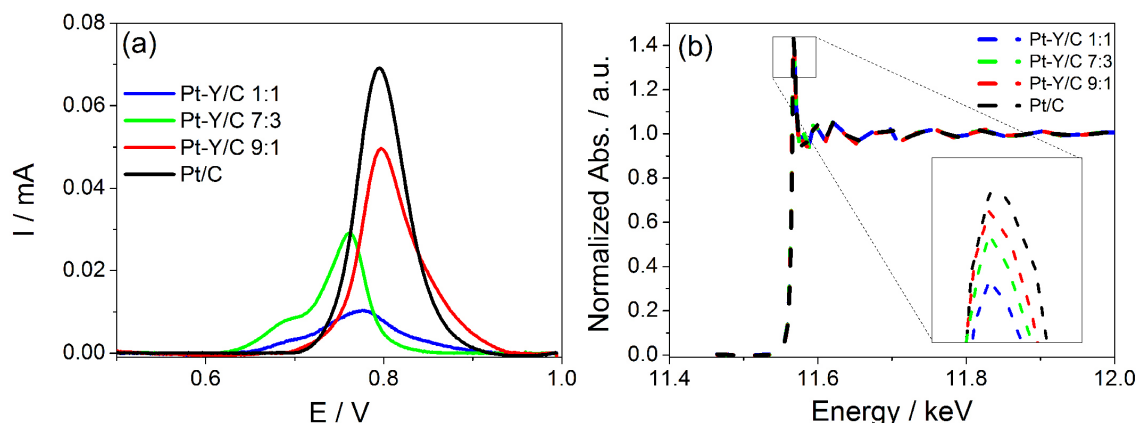


Figure 6. CO stripping profile in 0.5 M H_2SO_4 for Pt-Y/C catalysts (a) and XANES spectra at the Pt L_{III} edge for varying Pt:Y ratio and Pt/C (b).

accelerated aging test. Voltammetric profile and ORR polarization curves before and after the 3000 CV cycle aging test are shown in Figures 7a and 7b for Pt-Y/C. From Figure 7a we observe that the charge associated to adsorption/desorption of oxygenated specimens slightly decreases, while the hydrogen region remained practically the same after the aging test. Jeon and McGinn¹¹ observed an increase in current density in the hydrogen region corresponding to PtY and Pt_3Y catalyst after few voltammetric cycles. The authors attributed this behavior to yttrium dissolution.¹¹

The bar graph in Figure 7c illustrates the ORR activity loss of the Pt-Y/C 7:3 and Pt/C materials expressed in terms

of the specific activity at 0.9 V. The Pt/C catalyst exhibited a decrease in performance close to that of Pt-Y/C 7:3, in the order of 35%.

There are four mechanisms that are mainly responsible for the degradation of platinum nanoparticles electrocatalysts supported on carbon: (i) migration and coalescence of crystallites forming bigger particles on the carbon support, (ii) platinum dissolution and redeposition in bigger particles, known as the Ostwald Ripening process, (iii) platinum dissolution into the electrolyte, and (iv) release and agglomeration of nanoparticles due to carbon oxidation.^{40,41} The aging test conditions do not favor carbon support oxidation, so a combination of the first three

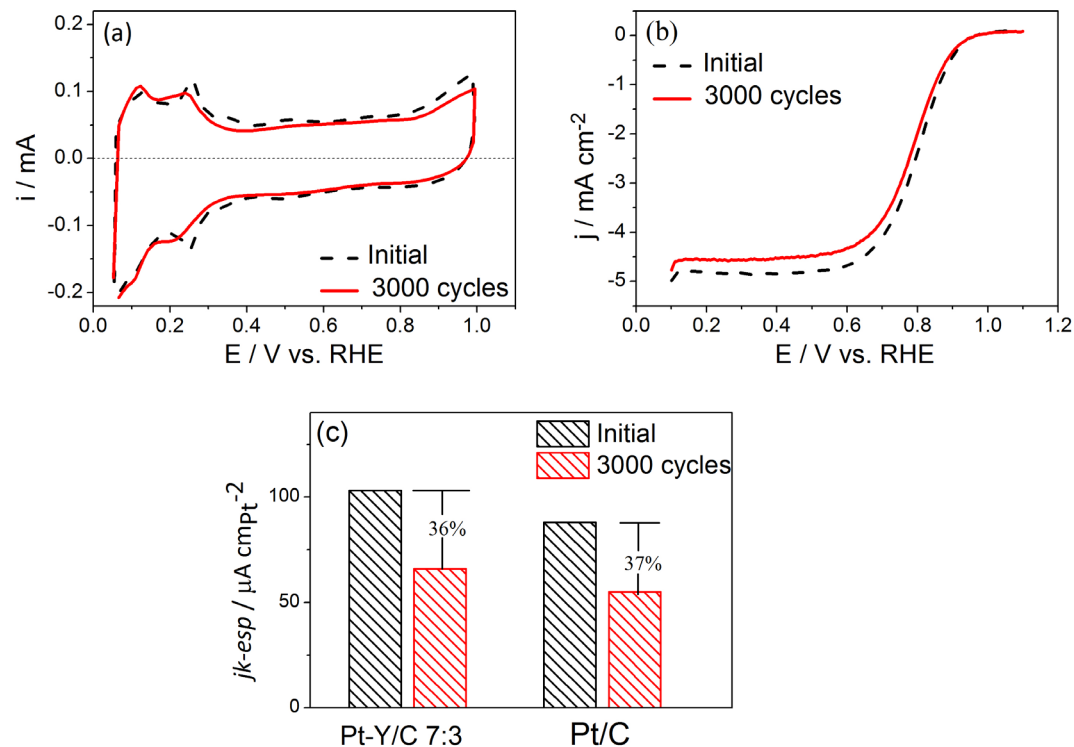


Figure 7. Comparison of cyclic voltammograms (a), ORR polarization curves obtained before and after 3000 CV cycle aging test for Pt-Y/C 7:3 catalyst (b) and ORR specific activity (jk_{esp}) loss, at 0.9 V, for Pt-Y/C 7:3 and Pt/C catalysts after 3000 CV cycle aging test (c).

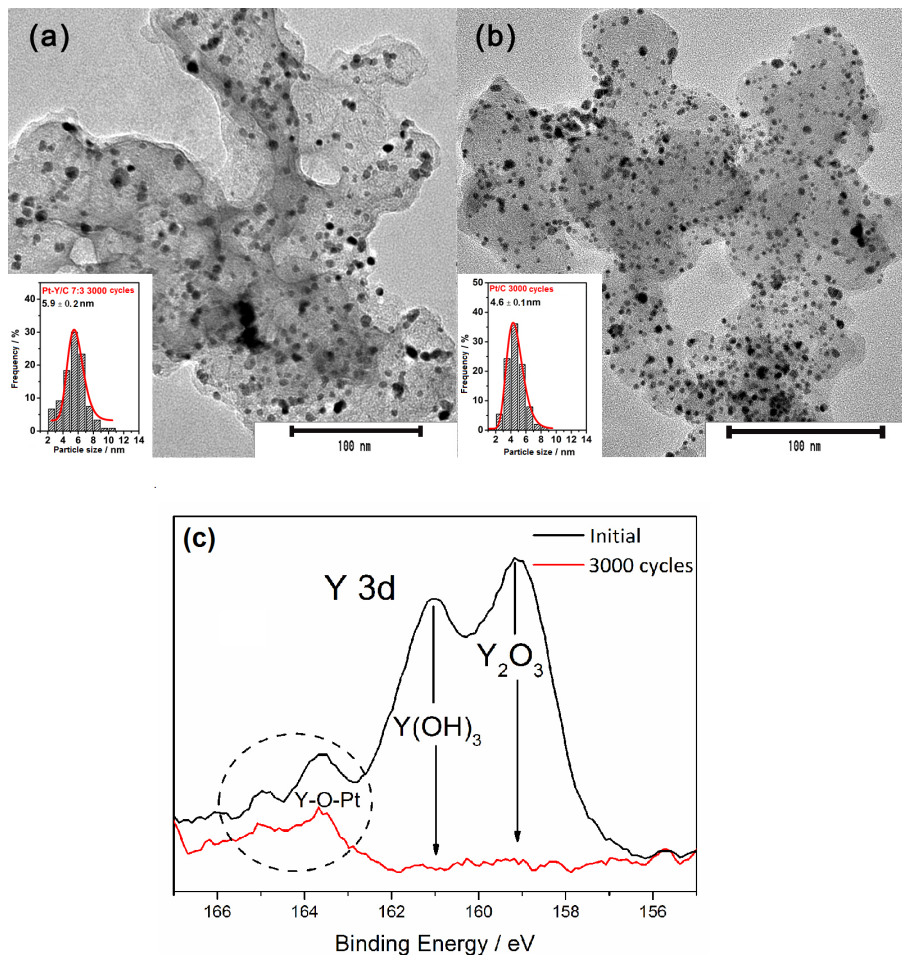


Figure 8. Electron micrographs and histograms of aged Pt-Y/C 7:3 (a) and Pt/C (b). XPS spectra of Pt-Y/C 7:3 ultrathin catalyst layer before and after 3000 cycles aging test (c).

mechanisms may be the cause of the catalyst degradation. The TEM micrographs of the aged materials are shown in Figure 8. The catalysts micrographs demonstrate a slightly increase of particle size for the Pt/C in comparison to that shown in Figure 1, while the mean particle size of the aged Pt-Y/C 7:3 remain unchanged. The mean particle sizes of the aged materials can be seen in Table 1.

Yttrium dissolution can be another contribution for the catalyst activity degradation. The atomic composition of ultrathin catalyst layer before and after the accelerated aging test was determined by EDS analysis. Before any electrochemical measurements, the atomic content of Pt and Y in the catalyst layer was equal to 69 and 31%, similar to the values determined for the as prepared Pt-Y/C 7:3 material. After the measurements, the yttrium content fell to 10%, proving that the metal undergoes dissolution.

Although some studies^{8,9,39} have shown that sputtering Pt-Y catalysts are stable after accelerated aging tests, Hernandez-Fernandez *et al.*⁴² observed that before electrochemical measurements the metals Pt and Y were equally distributed along the nanoparticles, while after

ORR measurements a core-shell structure was formed due to yttrium dissolution.⁴²

The catalytic layer deposited on the RDE was also evaluated using XPS technique. Figure 8c presents the high resolution XPS spectra before any electrochemical measurements and after the aging test for the binding energy region corresponding to the yttrium 3d transition. The initial spectrum of ultrathin catalyst layer is similar to that of the as prepared material shown in Figure 3. After the 3000 cycles aging test, the intensities of the Y 3d peaks are suppressed relative to the initial sample, agreeing with EDS analysis result. This result suggests that yttrium in the form of Y₂O₃ and Y(OH)₃ were dissolved, whereas the species Y-O-Pt is still in the catalyst.

Conclusions

Pt-Y/C electrocatalysts were prepared successfully by the modified formic acid method in different compositions. XRD analysis showed that no alloy was formed between the metals and XPS experiments showed that yttrium

is presented as Y_2O_3 , Y(OH)_3 and $\text{Y}-\text{O}-\text{Pt}$ species. CO stripping voltammograms confirmed that an interaction between Y and Pt nanoparticles occurs, whereas XAS experiments revealed a decrease in the white line intensity for Pt-Y/C electrocatalysts, indicating a modification on the Pt electronic structure. The specific activity for oxygen reduction reaction were compared and followed the sequence: Pt-Y (7:3) > Pt/C > Pt-Y (9:1) > Pt-Y (1:1), with the binary catalysts Pt-Y/C 7:3 ($103 \mu\text{A cm}_{\text{Pt}}^{-2}$) almost 20% higher than Pt/C ($88 \mu\text{A cm}_{\text{Pt}}^{-2}$).

The stability measurements for the Pt/C and Pt-Y/C 7:3 showed that: (i) Pt/C particle size slightly increased and that for Pt-Y/C 7:3 remained the same, corroborating with the small variation in the A_{esca} observed for both catalysts; (ii) EDS and XPS made in ultrathin catalyst layer showed a decrease in the amount of yttrium, and XPS revealed that only the species $\text{Y}-\text{O}-\text{Pt}$ still remain in the catalyst.

Despite the observed changes, Pt-Y/C catalytic activity decreases in the same proportion to the Pt catalyst, but remains higher. These results suggest that the species $\text{Y}-\text{O}-\text{Pt}$ might be partially responsible for maintaining higher activity of the catalyst. However, strategies that seek to maintain the integrity of the catalyst need to be designed with a view to commercial application in PEMFC.

Acknowledgments

The authors thank the grant 2011/50727-9 and 2013/17549-5, São Paulo Research Foundation (FAPESP) and CNPq (grant 307623/2012-2). The authors also wish to thank Brazilian Nanotechnology National Laboratory (LNNano) for assisting with the XPS measurements (Project 17696) and Brazilian Synchrotron Light Laboratory (LNLS) for assisting with the XAS experiments (Project 16866).

References

1. Stambouli, A. B.; *Renewable Sustainable Energy Rev.* **2011**, *15*, 4507. [Crossref]
2. Wang, Y.; Chen, K. S.; Mishler, J.; Cho, S. C.; Adroher, X. C.; *Appl. Energy* **2011**, *88*, 981. [Crossref]
3. Yano, H.; Kataoka, M.; Yamashita, H.; Uchida, H.; Watanabe, M.; *Langmuir* **2007**, *23*, 6438. [Crossref]
4. Malheiro, A. R.; Perez, J.; Villullas, H. M.; *J. Power Sources* **2010**, *195*, 3111. [Crossref]
5. Mani, P.; Srivastava, R.; Strasser, P.; *J. Phys. Chem. C* **2008**, *112*, 2770. [Crossref]
6. Lim, B.; Jiang, M.; Camargo, P. H. C.; Cho, E. C.; Tao, J.; Lu, X.; Zhu, Y.; Xia, Y.; *Science* **2009**, *324*, 1302. [Crossref]
7. Zhao, D.; Yan, B.; Xu, B.-Q.; *Electrochim. Commun.* **2008**, *10*, 884. [Crossref]
8. Greeley, J.; Stephens, I. E. L.; Bondarenko, A. S.; Johansson, T. P.; Hansen, H. A.; Jaramillo, T. F.; Rossmeisl, J.; Chorkendorff, I.; Nørskov, J. K.; *Nat. Chem.* **2009**, *1*, 552. [Crossref]
9. Stephens, I. E. L.; Bondarenko, A. S.; Bech, L.; Chorkendorff, I.; *ChemCatChem* **2012**, *4*, 341. [Crossref]
10. Yoo, S. J.; Kim, S.-K.; Jeon, T.-Y.; Hwang, S. J.; Lee, J.-G.; Lee, S.-C.; Lee, K.-S.; Cho, Y.-H.; Sung, Y.-E.; Lim, T.-H.; *Chem. Commun.* **2011**, *47*, 11414. [Crossref]
11. Jeon, M. K.; McGinn, P. J.; *J. Power Sources* **2011**, *196*, 1127. [Crossref]
12. Nishanth, K. G.; Sridhar, P.; Pitchumani, S.; *Electrochim. Commun.* **2011**, *13*, 1465. [Crossref]
13. Luo, Y.; Habrioux, A.; Calvillo, L.; Granozzi, G.; Alonso-Vante, N.; *ChemPhysChem* **2014**, *15*, 2136. [Crossref]
14. Luo, Y.; Habrioux, A.; Calvillo, L.; Granozzi, G.; Alonso-Vante, N.; *ChemCatChem* **2015**, *7*, 1573. [Crossref]
15. Gonzalez, E. R.; Ticianelli, E. A.; Pinheiro, A. L. N.; Perez, J.; *BR-SP 00321 1997*.
16. dos Santos, L.; Colmati, F.; Gonzalez, E. R.; *J. Power Sources* **2006**, *159*, 869. [Crossref]
17. Markovic, N.; Gasteiger, H.; Ross, P. N.; *J. Electrochim. Soc.* **1997**, *144*, 1591. [Crossref]
18. Kinoshita, K.; *J. Electrochim. Soc.* **1990**, *137*, 845. [Crossref]
19. Shao, M.; Peles, A.; Shoemaker, K.; *Nano Lett.* **2011**, *11*, 3714. [Crossref]
20. McBreen, J.; O'Grady, W. E.; Pandya, K. I.; Hoffman, R. W.; Sayers, D. E.; *Langmuir* **1987**, *3*, 428. [Crossref]
21. Biegler, T.; Rand, D. A. J.; Woods, R.; *J. Electroanal. Chem. Interfacial Electrochem.* **1971**, *29*, 269. [Crossref]
22. Opekar, F.; Beran, P.; *J. Electroanal. Chem. Interfacial Electrochem.* **1976**, *69*, 1. [Crossref]
23. Carmo, M.; dos Santos, A. R.; Poco, J. G. R.; Linardi, M.; *J. Power Sources* **2007**, *173*, 860. [Crossref]
24. Mukerjee, S.; Srinivasan, S.; Soriaga, M. P.; McBreen, J.; *J. Phys. Chem.* **1995**, *99*, 4577. [Crossref]
25. Carmo, M.; Paganin, V. A.; Rosolen, J. M.; Gonzalez, E. R.; *J. Power Sources* **2005**, *142*, 169. [Crossref]
26. Xu, Z.; Li, C.; Cheng, Z.; Zhang, C.; Li, G.; Peng, C.; Lin, J.; *Cryst. Eng. Comm.* **2010**, *12*, 549. [Crossref]
27. Cullity, B. D.; *Wesley Mass.* **1978**, 127.
28. Patterson, A. L.; *Phys. Rev.* **1939**, *56*, 978. [Crossref]
29. Palenzona, A.; Cirafici, S.; *J. Phase Equilib.* **1990**, *11*, 493. [Crossref]
30. Moulder, J. F.; Stickle, W. F.; Sobol, P. E.; Bomben, K. D.; *Handbook of X-ray Photoelectron Spectroscopy*; Chastain, J., ed.; Perkin-Elmer Corporation: Eden Prairie, 1992.
31. Mongstad, T.; Thøgersen, A.; Subrahmanyam, A.; Karazhanov, S.; *Sol. Energy Mater. Sol. Cells* **2014**, *128*, 270. [Crossref]
32. Gougousi, T.; Chen, Z.; *Thin Solid Films* **2008**, *516*, 6197. [Crossref]

33. Ting, C.-C.; Tsai, C.-H.; Chien, Y.-C.; Yu, C.-T.; *J. Electrochem. Soc.* **2012**, *159*, H400. [Crossref]
34. Schwämmlein, J. N.; Harzer, G. S.; Pfändner, P.; Blankenship, A.; El-Sayed, H. A.; Gasteiger, H. A.; *J. Electrochem. Soc.* **2018**, *165*, J3173. [Crossref]
35. Brandiele, R.; Guadagnini, A.; Girardi, L.; Dražić, G.; Dalconi, M. C.; Rizzi, G. A.; Amendola, V.; Durante, C.; *Catal. Sci. Technol.* **2020**, *10*, 4503. [Crossref]
36. Tsuji, M.; Uto, K.; Nagami, T.; Muto, A.; Fukushima, H.; Hayashi, J.; *ChemCatChem* **2017**, *9*, 962. [Crossref]
37. Corradini, P. G.; Antolini, E.; Perez, J.; *Phys. Chem. Chem. Phys.* **2013**, *15*, 11730. [Crossref]
38. Lin, R.; Cao, C.; Zhang, H.; Huang, H.; Ma, J.; *Int. J. Hydrogen Energy* **2012**, *37*, 4648. [Crossref]
39. Yoo, S. J.; Lee, K.-S.; Hwang, S. J.; Cho, Y.-H.; Kim, S.-K.; Yun, J. W.; Sung, Y.-E.; Lim, T.-H.; *Int. J. Hydrogen Energy* **2012**, *37*, 9758. [Crossref]
40. Dubau, L.; Castanheira, L.; Berthomé, G.; Maillard, F.; *Electrochim. Acta* **2013**, *110*, 273. [Crossref]
41. Sugawara, Y.; Yadav, A. P.; Nishikata, A.; Tsuru, T.; *J. Electroanal. Chem.* **2011**, *662*, 379. [Crossref]
42. Hernandez-Fernandez, P.; Masini, F.; McCarthy, D. N.; Strelbel, C. E.; Friebel, D.; Deiana, D.; Malacrida, P.; Nierhoff, A.; Bodin, A.; Wise, A. M.; Nielsen, J. H.; Hansen, T. W.; Nilsson, A.; Stephens, I. E. L.; Chorkendorff, I.; *Nat. Chem.* **2014**, *6*, 732. [Crossref]

Submitted: July 15, 2022

Published online: October 14, 2022



This is an open-access article distributed under the terms of the Creative Commons Attribution License.